LAWRENCE
LIVERMORE
NATIONAL
LABORATORY

LLNL-CONF-407792

Demonstration of ITER Operational Scenarios on DIII-D

E. J. Doyle, R. V. Budny, J. C. DeBoo, J. R. Ferron, G. L. Jackson, T. C. Luce, M. Murakami, T. H. Osborne, J.-M. Park, P. A. Politzer, H. Reimerdes, T. A. Casper, C. D. Challis, R. J. Groebner, C. T. Holcomb, A. W. Hyatt, R. J. La Haye, G. R. McKee, T. W. Petrie, C. C. Petty, T. L. Rhodes, M. W. Shafer, P. B. Snyder, E. J. Strait, M. R. Wade, G. Wang, W. P. West, L. Zeng

October 14, 2008

22nd IAEA-FEC
Geneva, Switzerland
October 13, 2008 through October 18, 2008

Disclaimer

This document was prepared as an account of work sponsored by an agency of the United States government. Neither the United States government nor Lawrence Livermore National Security, LLC, nor any of their employees makes any warranty, expressed or implied, or assumes any legal liability or responsibility for the accuracy, completeness, or usefulness of any information, apparatus, product, or process disclosed, or represents that its use would not infringe privately owned rights. Reference herein to any specific commercial product, process, or service by trade name, trademark, manufacturer, or otherwise does not necessarily constitute or imply its endorsement, recommendation, or favoring by the United States government or Lawrence Livermore National Security, LLC. The views and opinions of authors expressed herein do not necessarily state or reflect those of the United States government or Lawrence Livermore National Security, LLC, and shall not be used for advertising or product endorsement purposes.

Demonstration of ITER Operational Scenarios on DIII-D

E.J. Doyle 1), R.V. Budny 2), J.C. DeBoo 3), J.R. Ferron 3), G.L. Jackson 3), T.C. Luce 3), M. Murakami 4), T.H. Osborne 3), J.-M. Park 4), P.A. Politzer 3), H. Reimerdes 5), T.A. Casper 6), C.D. Challis 7), R.J. Groebner 3), C.T. Holcomb 6), A.W. Hyatt 3), R.J. La Haye 3), G.R. McKee 8), T.W. Petrie 3), C.C. Petty 3), T.L. Rhodes 1), M.W. Shafer 8), P.B. Snyder 5), E.J. Strait 3), M.R. Wade 3), G. Wang 1), W.P. West 3), and L. Zeng 1)

1) Physics Dept. and PSTI, University of California, Los Angeles, California 90095, USA
2) Princeton Plasma Physics Laboratory, Princeton, New Jersey, USA
3) General Atomics, P.O. Box 85608, San Diego, California 92186-5608, USA
4) Oak Ridge National Laboratory, Oak Ridge, Tennessee, USA
5) Columbia University, New York, New York, USA
6) Lawrence Livermore National Laboratory, Livermore, California, USA
7) Euratom/UKAEA Fusion Association, Culham Science Centre, Oxon OX14 3DB, UK
8) University of Wisconsin-Madison, Madison, Wisconsin, USA

e-mail contact of main author: edoyle@ucla.edu

Abstract. The DIII-D program has recently initiated an effort to provide suitably scaled experimental evaluations of four primary ITER operational scenarios. New and unique features of this work are that the plasmas incorporate essential features of the ITER scenarios and anticipated operating characteristics; e.g., the plasma cross-section, aspect ratio and value of I/aB of the DIII-D discharges match the ITER design, with size reduced by a factor of 3.7. Key aspects of all four scenarios, such as target values for β_N and H_{98}, have been replicated successfully on DIII-D, providing an improved and unified physics basis for transport and stability modeling, as well as for performance extrapolation to ITER. In all four scenarios normalized performance equals or closely approaches that required to realize the physics and technology goals of ITER, and projections of the DIII-D discharges are consistent with ITER achieving its goals of ≥400 MW of fusion power production and $Q \geq 10$. These studies also address many of the key physics issues related to the ITER design, including the L-H transition power threshold, the size of ELMs, pedestal parameter scaling, the impact of tearing modes on confinement and disruptivity, beta limits and the required capabilities of the plasma control system. An example of direct influence on the ITER design from this work is a modification of the specified operating range in internal inductance at 15 MA for the poloidal field coil set, based on observations that the measured inductance in the baseline scenario case lay outside the original ITER specification.

1. Introduction

It is critical to the future success of the US and worldwide fusion programs that the ITER tokamak [1] meet its physics and technology goals. The expected future performance of ITER can be investigated on present devices via experiments which match absolute or normalized ITER plasma parameters, e.g. [2–7]. Towards this end, the DIII-D program has recently initiated an effort to provide suitably scaled experimental evaluations of four primary ITER operational scenarios. New and unique features of this work are that the plasmas incorporate essential operational features of the ITER scenarios, such as the design values for the ITER plasma cross-section and aspect ratio. Evaluation of all four ITER scenarios on a single tokamak enables direct cross-comparisons of performance and operational issues. The four ITER scenarios [1] which have been demonstrated are: the baseline or reference scenario, which targets a fusion gain factor (Q) of 10 using a conventional ELMing H-mode discharge at 15 MA plasma current; the hybrid scenario, which targets a high neutron fluence mission at reduced plasma current (~12 MA), operating with enhanced confinement and stability; the steady-state scenario, which seeks fully noninductive (NI) operation at lower plasma currents (~9 MA), again employing enhanced

confinement and stability in order to obtain a target Q~5; and the "advanced inductive" (AI) scenario, which targets ITER's goals of investigating ignited or near-ignited plasmas (Q≥20) and 700 MW fusion power output by combining full current operation with the increased plasma confinement and stability limits characteristic of hybrid operation. Key aspects of all four of these scenarios have been replicated successfully on DIII-D, providing an improved and unified physics basis for transport and stability modeling, as well as performance extrapolation to ITER. In all four scenarios performance equals or closely approaches that required to realize the physics and technology goals of ITER.

That plasma shaping plays a significant role in determining plasma stability limits, confinement and pedestal properties is well understood [8–10], and both modeling and experiment indicate that the edge plasma stability is sensitive to small variations in plasma shape [10]. Consequently, all four scenarios were operated on DIII-D with a version of the ITER plasma scaled by a factor of 3.7, as shown in Fig. 1, maintaining the design values for the ITER plasma cross-section and aspect ratio of 3.1. Operating with the correct ITER plasma cross-section and aspect ratio is a unique feature of this work.

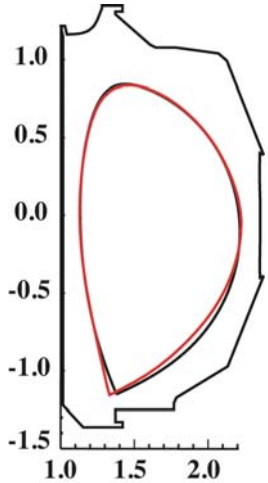

FIG. 1. Comparison of scaled ITER plasma cross-section (black) and experimental DIII-D plasma cross-section (red).

These demonstrations focus on the current flat-top phase of the discharges; in general no attempt was made to simulate ITER startup prescriptions and constraints, which were addressed in separate work [11,12]. The demonstration discharges were operated with predominant co-NBI, driving significant plasma toroidal rotation which is known to affect confinement, e.g. [13]. In addition, not all of the scenarios were operated with T_i=T_e, as anticipated on ITER. These issues, and others such as shape sensitivity studies, will be addressed in future work.

2. DIII-D Realizations of ITER Operating Scenarios and Projections to ITER

The basic parameters obtained for the four ITER scenarios evaluated on DIII-D are presented here. Unless otherwise noted, all plasmas were run at a common magnetic field of 1.9 T, in order to facilitate direct comparisons on DIII-D, and to anticipated operating scenarios at fixed (full) field on ITER. Projections of the DIII-D results to fusion power output (P_{fus}) and Q on ITER are made using a spreadsheet model which implements the methodology described in [4]. The projections to ITER are made for the same β_N as achieved on DIII-D, using the DIII-D electron temperature profile and with T_i=T_e, but with the density profile scaled to give n_e=0.85n_G, where $n_G \equiv I/\pi a^2$ (10^{20} m^{-3}, MA, m) is the Greenwald density. Three different confinement scalings are used in making the projections: the L-mode ITER-89P scaling (confinement scaling factor denoted by H_{89}) [14], which is Bohm-like; a pure gyroBohm (DS03) scaling derived from the ITER database [15]; and the ITER H-mode scaling, IPB98y2 (confinement factor denoted by H_{98}) [16], which has an intermediate character between Bohm and gyroBohm. These projections and the plasma parameters achieved for the four scenarios described below are summarized in Table I.

Baseline or reference scenario. Conventional ELMy H-mode plasmas have been operated at a normalized current $I_N \equiv I/aB$ (MA, m, T) value of 1.415, corresponding to 15 MA operation on ITER. Use of I_N allows a definite translation of plasma current from ITER to DIII-D, given the same plasma shape. The resulting value of q_{95} is 3.1, close to the ITER design value of 3.0. The plasma was operated with feedback control of the NBI power

so as to maintain the ITER target value of β_N=1.8. The time evolution of the main plasma parameters for such a discharge is illustrated in Fig. 2, while profiles are shown in Fig. 3. As can be seen, confinement is at or above the ITER target of H_{98}=1.0, and the density is high, increasing up to the ITER absolute target density of 1.0x10^{20} m^{-3}, or ~0.65n_G on DIII-D. NTM activity is present and decreases confinement by ~10%, while many of these discharges disrupt due to mode locking. The parameter $G \equiv \beta_N H_{89}/q_{95}^2$ [4], a measure of the normalized fusion performance, is close to the 0.42 level predicted for Q=10 operation on ITER (much of the difference is due to the fact that q_{95} is not 3.0 as assumed for ITER). As shown in Table I, however, the more detailed spreadsheet model projects that this discharge meets or exceeds the ITER targets of 400 MW of fusion power and $Q \geq 10$ for this scenario, for all three confinement scalings utilized. Two other major features of these discharges are also evident in Fig. 2: The baseline discharges exhibit large and infrequent Type I ELMs, leading to poor density control. In general, the ELMs are not synchronous with the sawteeth present in the discharge (Fig. 8). In addition, the 3 s H-mode period corresponds to ~3τ_R, or approximately the same normalized duration as anticipated on ITER. However, the discharges are non-stationary, as is evident in the increase in density and decline in confinement with time (Fig. 2), and also in the fact that the plasma internal inductance continually declines during the H-mode period (not shown).

TABLE I. Parameters at full performance for the four operating scenarios.

	Baseline (131498)	Hybrid (DIII-D Startup, 131711)	Hybrid (ITER Startup, 131265)	Advanced Inductive (133137)	Steady State (131198)
β_N, β_p	1.8, 0.65	2.2, 1.1	2.8, 1.3	2.8, 1.05	3.0, 1.6
Equivalent ITER I_p (MA)	15.0	11.4	11.2	14.8	10.7
q_{95}	3.1	4.3	4.1	3.3	4.7
H_{89}, H_{98}	2.0, 1.1	2.6, 1.5	2.5, 1.45	2.4, 1.5	2.2, 1.46
G	0.37	0.31	0.4	0.6	0.3
B (T), I_p (MA)	1.92, 1.47	1.92, 1.13	2.11, 1.28	1.93, 1.49	1.92, 1.05
n (10^{19} m^{-3}), n/n_G	8–10, 0.5–0.65	6.6, 0.55	5.3, 0.41	5.3, 0.35	4.7, 0.4
P_{aux} (MW)	3.5	3.47	8.0	7.7	9.38
τ_E (s)	0.22	0.24	0.17	0.18	0.115
$v_\phi(0)$ (km/s), $M_\phi(0)$	140, 0.26	220, 0.4	290, 0.36	220, 0.3	190, 0.4
$\langle p \rangle \tau_E$ (kPa-s)	8.1	8.4	9.7	10.4	5.3
Z_{eff}	3.0	2.9	1.9	1.8	1.9
Averaging time (s)	2.6–3.6	2.85–3.45	2.8–3.3	2.8–3.8	3.4–3.9
P_{fus} (MW) (89P, 98y2, DS03)	443, 427, 404	382, 371, 329	532, 477, 432	818, 723, 723	532, 502, 452
Q (89P, 98y2, DS03)	10.3, 22.4, ∞	6.3, 10.2, ∞	5.8, 23.3, ∞	13.5, ∞, ∞	2.7, 5.8, 19.8
Auxiliary heating	NBI	NBI	NBI	NBI	NBI + off-axis ECCD
Internal MHD	Sawteeth, n=2 tearing	Sawteeth, n=2 tearing	Fishbones, n=3 tearing	Sawteeth, n=3 tearing	n=3 tearing

Profiles for the baseline scenario, Fig. 3, show that $T_e \sim T_i$ across the plasma radius, as might be expected at such high operating densities. The ion thermal and neoclassical transport rates shown are calculated using the TRANSP code [17]. The density profile is substantially peaked, as against a flat density profile assumed in the standard ITER profile

models [18], but in qualitative agreement with recent AUG and JET observations and predictions of peaked density profiles [19].

Hybrid Scenario. Using the standard DIII-D prescription for hybrid operation [4], a limited number of discharges were operated at a current equivalent to 11.4 MA on ITER, with q_{95}=4.3. These discharges had a maximum sustained β_N of ~2.2, substantially less than normal for DIII-D hybrid plasmas [5]. However, discharges run with the ITER "large-bore" startup prescription, with no heating during the current ramp phase and a slightly different version of the ITER shape, exhibited substantially higher performance. These discharges, with a current equivalent to 11.2 MA on ITER, q_{95}=4.1 and B_T=2.1 T, are described in detail in a companion paper [12], demonstrating sustained operation with β_N=2.8 and excellent confinement, H_{98}=1.45, comfortably exceeding the ITER targets [1] of 2.0–2.5 and 1.0–1.2, respectively. As compared with the baseline scenario, the hybrids operate at lower density, with higher rotation and T_i somewhat higher than T_e. Summary details for hybrid discharges with a DIII-D-like startup (131711) and an ITER-like startup (131265) are included in Table I. As can be seen, in addition to addressing the ITER hybrid mission, these discharges also offer a possible alternative route to achieving the ITER Q=10 mission, but at reduced current.

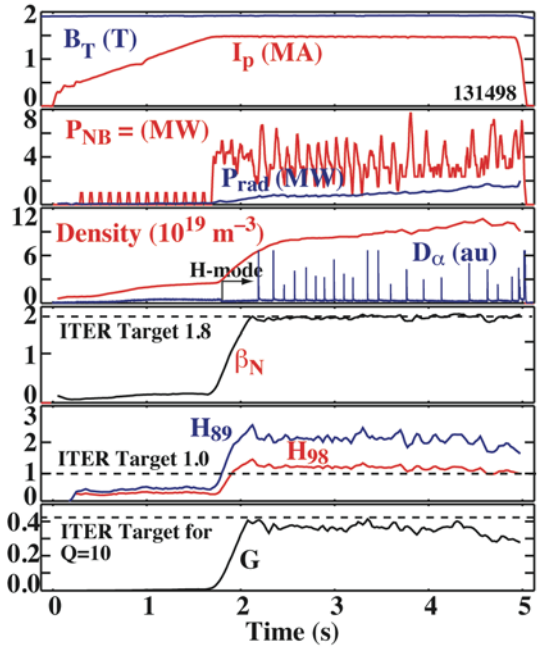

FIG. 2. Time evolution of key plasma parameters for baseline or reference scenario demonstration discharge 131498.

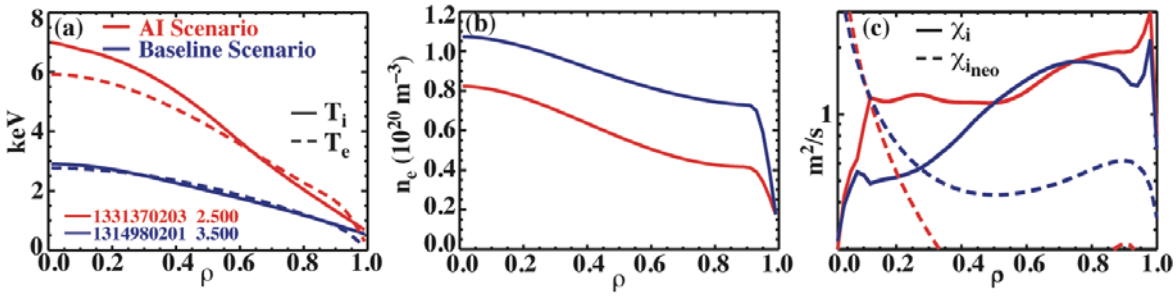

FIG. 3. Profiles for (a) T_i and T_e, (b) n_e, and (c) χ_i and neoclassical transport rates for baseline (131498, in blue) and advanced inductive (133137, in red) scenario discharges.

Advanced Inductive (AI) Scenario. These discharges utilized the standard DIII-D prescription for hybrid operation [4,5], but at higher current, equivalent to 14.8 MA on ITER, with q_{95}=3.3. As shown in Fig. 4, this combination resulted in a discharge exhibiting very high fusion performance, with β_N=2.8, H_{98}=1.5 and G=0.6. As compared with the baseline scenario, ELMs are more frequent and smaller, giving good density control. Profiles for this discharge are included in Fig. 3, where they can be compared to those of the baseline scenario discharge, e.g. T_e is still comparable to T_i. As seen in Table I, this discharge projects to very high performance on ITER, with >700 MW of fusion power and Q of ~13–∞, depending on the confinement scaling utilized.

Steady-state scenario. Steady-state demonstration discharges were operated using a standard DIII-D prescription [20,21], with early neutral beam heating to induce an L-H tran-

sition during the current-ramp phase. Off-axis current drive was provided by up to 3 MW of ECCD, using a relatively broad deposition profile to provide improved 2/1 NTM stability [21]. The discharges were operated over a range of plasma currents, corresponding to 8.5–10.8 MA operation on ITER, and q_{95} of 4.7–6.3, with an elevated q-profile, q_{min}≥1.5. At the lower current end of the range, full noninductive or overdriven operation was obtained, but with relatively low fusion performance. Conversely, at the upper end of the current range the discharges were not fully noninductive, but had higher fusion performance at the G~0.3 level predicted for Q~5 operation on ITER. Additional ECCD power is needed to increase the noninductive current fraction to 100% at the G~0.3 level, which will be available in the future on DIII-D. The time evolution of the main plasma parameters for an 8.5 MA equivalent discharge is illustrated in Fig. 5, while profiles are shown in Fig. 6. The surface loop voltage for this discharge is ±5 mV, consistent with full NI operation, while TRANSP analysis indicates overdrive after ~3 s, Fig. 5. As compared with the baseline discharges, Fig. 6, the lower densities associated with steady-state operation result in T_i>T_e. As shown in Table I, rotation is high in the steady-state discharges, which may influence transport via ExB shear. However, the data also show that confinement and transport rates are conventional, with H_{98}~1.0, which is thought to be due to NTM activity. The data illustrated in Table I are for one of the higher current (10.7 MA equivalent), higher fusion performance discharges.

For the scaled ITER shape shown in Fig. 1, the plasma-wall gap (i.e. plasma to first tile gap) at the outboard midplane is large, ~15 cm. With this large gap the maximum sustained β_N which could be operated was ~2.8, meeting the ITER target of β_N≥2.6. This value of β_N barely exceeds the ideal MHD n=1 no-wall limit as calculated with the DCON code [22]. At larger values of β_N, which can be accessed transiently, the amplification of an externally applied slowly rotating n=1 field rapidly increases, indicating a significant reduction in

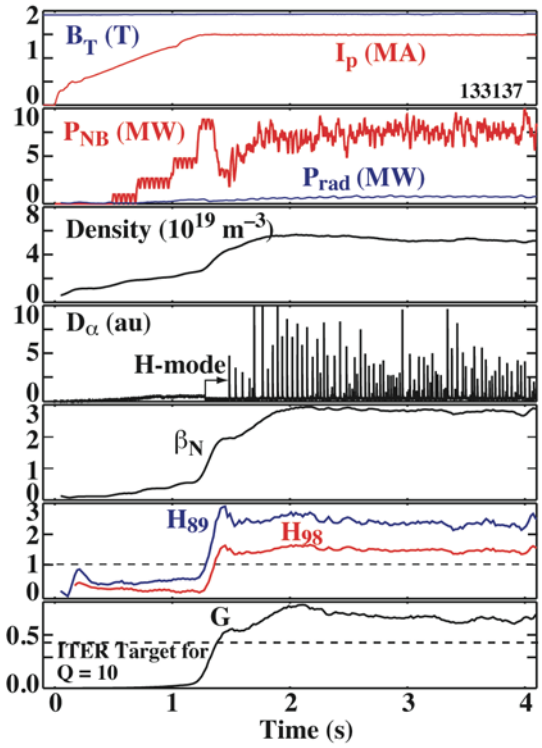

FIG. 4. Time evolution of key plasma parameters for advanced inductive scenario demonstration discharge 133137.

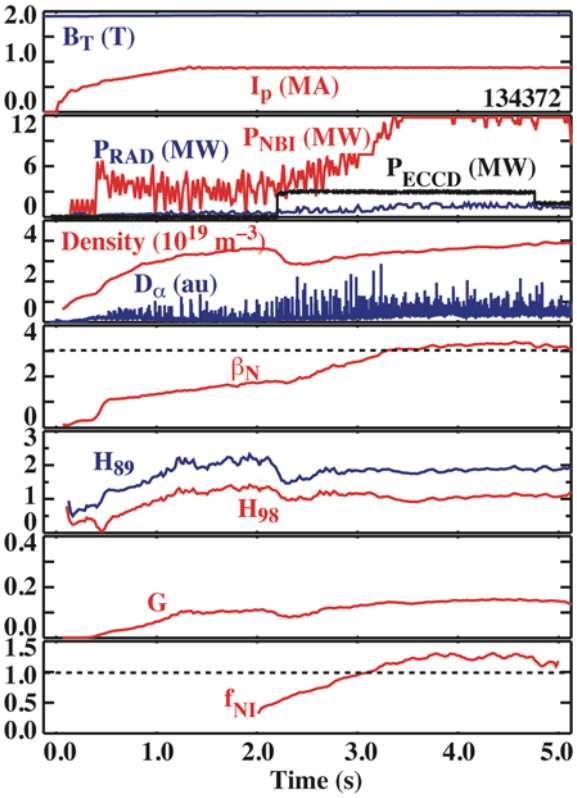

FIG. 5. Time evolution of key plasma parameters for steady-state scenario demonstration discharge 134372.

the stability of the n=1 kink mode [23]. However, by operating the discharges with a smaller size scaling factor of 3.48 (as opposed to 3.7), the outer gap was reduced to ~8.5 cm, a typical value for DIII-D AT discharges. With this reduced gap, wall stabilization was increased, and sustained plasma operation was achieved with β_N of 3.1–3.3, as shown in Fig. 5. The steady-state discharge listed in Table I (131198) had the larger outer-gap, as for the other scenarios.

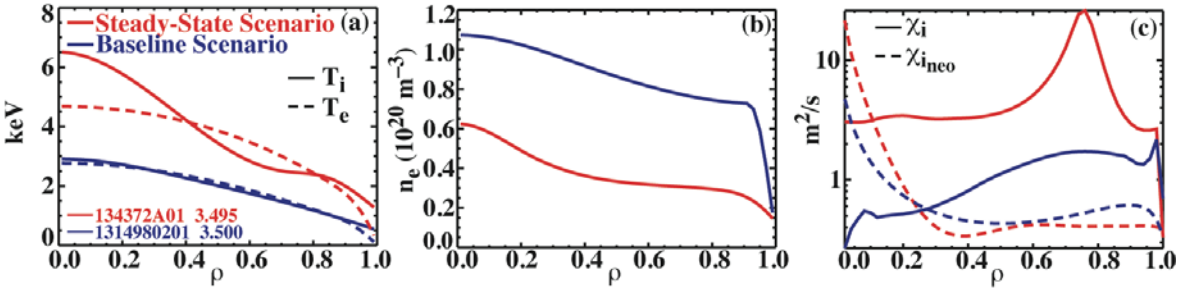

FIG. 6. Profiles for (a) T_i and T_e, (b) n_e, and (c) χ_i and neoclassical transport rates for steady-state (134372, in red) and baseline (131498, in blue) discharges.

3. ITER Physics Issues Illustrated by the Demonstration Discharges

A major benefit of the demonstration discharges is that they address many of the leading physics issues facing ITER. Among such issues encountered in the demonstration discharges are the L-H transition power threshold, the size and impact of ELMs, pedestal parameter scaling, the impact of tearing modes on confinement and disruptivity, beta limits and the required capabilities of the plasma control system. One area where the demonstration discharges have already had a significant impact on the ITER design is with regard to the required capabilities of the poloidal field coil system. ITER was originally designed for plasma internal inductances in the range 0.7–1.0 at 15 MA (ITER employs $l_i(3)$ as a measure of internal inductance, see [12]). However, as shown in Fig. 7, the measured values for $l_i(3)$ for all four scenarios evolve during the plasma flattop phase to values below 0.7, with some values as low as 0.5. Having $l_i(3)$ values outside the ITER design range would result in a loss of plasma shape control on ITER. In response to these results from DIII-D, and other devices [24], the operating range of the ITER shape control system is being expanded [25].

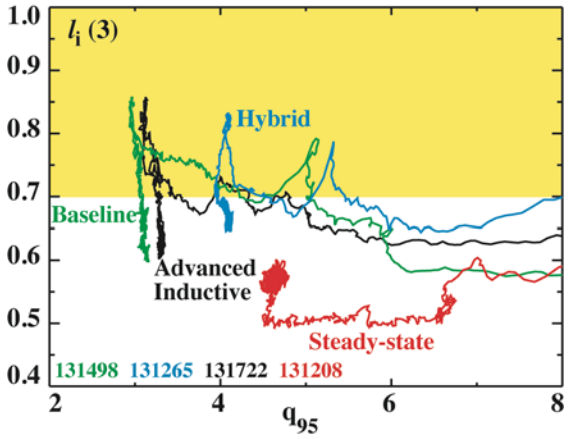

FIG. 7. Trajectories in $l_i(3)$ vs q_{95} space for each operating scenario. The discharges all begin at the right-hand side with high q_{95} and progress to the left. The yellow shaded region indicates the original ITER design range in $l_i(3)$.

Another key issue for ITER is that of achieving tolerable ELM characteristics. As part of the ITER design update process, the allowable limits for energy loss per ELM (ΔW_{ELM}) are being reduced to ≤1 MJ, or ≤1% of the pedestal energy [26]. The impact of individual ELMs on the plasma total stored energy and density in a DIII-D baseline scenario discharge is shown in detail in Fig. 8. As can be seen, each ELM causes a loss of ~15% of the total stored energy, and ~30% of the pedestal energy. This observed ΔW_{ELM} substantially exceeds the allowable ITER limits [26], and is also well above the standard scaling for ELM energy loss [27], indicating the critical need for a robust ELM suppression system on ITER. The fact that

these ELMs exceed the standard scaling is probably associated with their very large radial extent, into ρ~0.5 in the plasma pressure profile. Modeling with the ELITE code [28] is consistent with Type I ELM behavior governed by intermediate-n peeling ballooning stability, but with a wider radial eigenmode extent than usual.

The L-H transition in the baseline scenario discharges (Fig. 2) is triggered shortly after the application of a fixed NBI power of ~4.4 MW, which exceeds the threshold power (P_{thr}) as predicted by the latest scaling relation [29]. After the L-H transition, with the NBI under feedback control to maintain β_N=1.8, the ratio of the loss power (P_L) to P_{thr} declines as the density rises, down to ~0.8, and some of the discharges exhibit H-L back-transitions. [Note that this use of the scaling law to predict P_{thr} during the H-mode period is questionable as the scaling was derived specifically for the L-H transition, not the H-L back-transition.] However, a separate discharge with fixed input NBI power of 2.6 MW and a density of 4.0×10^{19} m^{-3} remained in L-mode for over a second with P_L/P_{thr}~2, until an L-H transition was eventually triggered by a sawtooth, i.e. the experimentally determined power threshold appears to be a factor of ~2 higher than the scaling prediction. The measured pedestal conditions in these ITER scenario plasmas are also being used as part of the experimental tests [30] of a new predictive model for the pedestal height, EPED1 [31]. Illustrated in Fig. 9 is a comparison of the edge pedestal for the four scenarios, showing good agreement between the measurements and the EPED1 model [30,31].

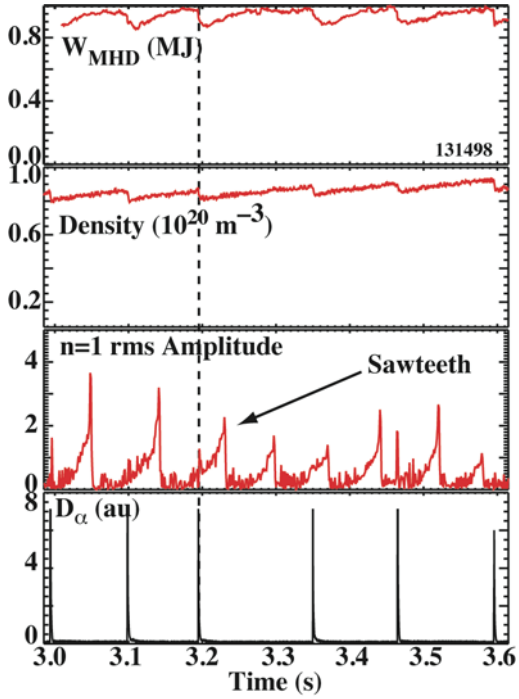

FIG. 8. Total stored energy and density variations induced by individual Type I ELMs in the baseline scenario discharge shown in Fig. 2 (131498).

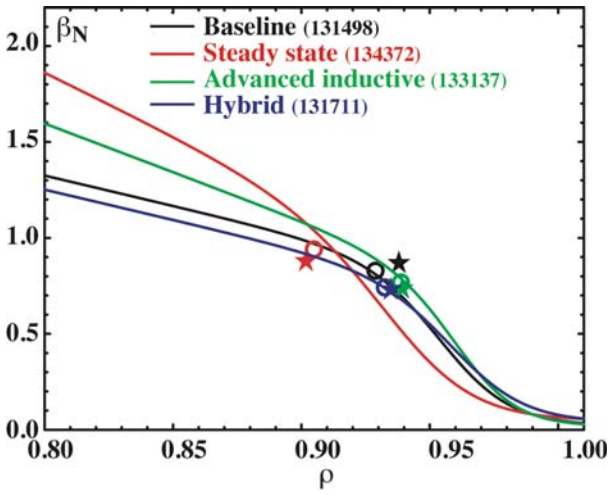

FIG. 9. H-mode edge pedestals for the four scenarios. The measured pedestal heights and widths are indicated by the open circles, while corresponding EPED1 model predictions are indicated by filled stars.

4. Conclusions

Four leading ITER operational scenarios have been successfully demonstrated on DIII-D, viz. the baseline, hybrid, advanced inductive and steady-state scenarios. The results of these demonstrations are uniformly positive with regard to ITER meeting its performance targets for fusion gain (Q) and fusion power production. The DIII-D discharges project to a fusion power output in the range of ~400–800 MW, with Q of ~5 to infinity, depending on scenario and confinement scaling utilized. The demonstration discharges also provide crucial information on many of the key physics issues facing ITER, such as ELM behavior and pedestal scaling, where the observations support the critical need for a robust

ELM suppression system on ITER. The DIII-D results have also directly influenced the evolution of the ITER design, having indicated the need for a broader operating range in internal inductance for the poloidal field coil set.

Acknowledgments

This work was supported in part by the US Department of Energy under DE-FG03-01ER54615, DE-AC02-76CH03073, DE-FC02-04ER54698, DE-AC05-00OR22725, DE-FG02-89ER53297, DE-AC52-07NA27344 at LLNL, and DE-FG02-89ER53296.

References

[1] Special issue on "Progress in the ITER Physics Basis," Nucl. Fusion **47**, S1 (2007).
[2] CORDEY, J.G., *et al.*, Plasma Phys. Control. Fusion **38**, 1237 (1996).
[3] KAMADA, Y., JT-60 Team, Nucl. Fusion **41**, 1311 (2001).
[4] LUCE, T.C., *et al.*, Phys. Plasmas **11**, 2627 (2004).
[5] WADE, M.R., *et al.*, Nucl. Fusion **45**, 407 (2005).
[6] JOFFRIN, E., *et al.*, Nucl. Fusion **45**, 626 (2005).
[7] PETTY, C.C., Fusion Sci. Technol. **48**, 978 (2005).
[8] FERRON, J.R., *et al.*, Phys. Plasmas **12**, 056126 (2005).
[9] GATES, D.A., *et al.*, Phys. Plasmas **13**, 056122 (2006).
[10] LEONARD, A.W., *et al.*, Phys. Plasmas **15**, 056114 (2008).
[11] JACKSON, G.L., *et al.*, submitted to Nucl. Fusion (2008).
[12] JACKSON, G.L., *et al.*, Fusion Energy 2008 (Proc. 22nd Int. Conf. Geneva, 2008) (Vienna: IAEA) CD-ROM file IT/P7-2.
[13] POLITZER, P.A., *et al.*, Nucl. Fusion **48**, 075001 (2008).
[14] YUSHMANOV, P.N., *et al.*, Nucl. Fusion **30**, 1999 (1990).
[15] PETTY, C.C., *et al.*, Fusion Sci. Technol. **43**, 1 (2003).
[16] ITER PHYSICS BASIS EDITORS, *et al.*, Nucl. Fusion **39**, 2137 (1999).
[17] HAWRYLUK, R.J., *Proc. Course in Physics Close to Thermonuclear Conditions (Varenna, 1979),* Vol. 1, p. 19 (Brussels, CEC, 1980).
[18] POLEVOI, A.R., *et al.*, Nucl. Fusion **45**, 1451 (2005).
[19] ANGIONI, C. *et al.*, Phys. Plasmas **14**, 055905 (2007).
[20] MURAKAMI, M., *et al.*, Phys. Plasmas **13**, 056106 (2006).
[21] FERRON, J.R., *et al.*, Fusion Energy 2008 (Proc. 22nd Int. Conf. Geneva, 2008) (Vienna: IAEA) CD-ROM file EX/P4-27.
[22] GLASSER A., and CHANCE, M.S., Bull. Am. Phys. Soc. **42**, 1848 (1997).
[23] REIMERDES, H. *et al.*, Phys. Rev. Lett. **93**, 135002 (2004).
[24] SIPS, A.C.C., *et al.*, Fusion Energy 2008 (Proc. 22nd Int. Conf. Geneva, 2008) (Vienna: IAEA) CD-ROM file IT/2-2.
[25] HAWRYLUK, R.J., *et al.*, Fusion Energy 2008 (Proc. 22nd Int. Conf. Geneva, 2008) (Vienna: IAEA) CD-ROM file IT/1-2.
[26] LOARTE, A., *et al.*, Fusion Energy 2008 (Proc. 22nd Int. Conf. Geneva, 2008) (Vienna: IAEA) CD-ROM file IT/P6-13.
[27] LOARTE, A., *et al.*, J. Nucl. Mater. **313-316**, 962 (2003).
[28] SNYDER, P.B. *et al.*, Phys. Plasmas **9**, 2037 (2002).
[29] MARTIN, Y.R., *et al.*, J. Phys: Conf. Series **123**, 012033 (2008).
[30] GROEBNER, R.J. *et al.*, Fusion Energy 2008 (Proc. 22nd Int. Conf. Geneva, 2008) (Vienna: IAEA) CD-ROM file EX/P3-5.
[31] SNYDER, P.B., *et al.*, Fusion Energy 2008 (Proc. 22nd Int. Conf. Geneva, 2008) (Vienna: IAEA) CD-ROM file IT/P6-14.